HHS Public Access

Author manuscript

J Physiol. Author manuscript.

The structural and functional effects of myosin regulatory light chain phosphorylation are amplified by increases in sarcomere length and [Ca^{2+}]

Kyrah L. Turner[1], **Blake J. Vander Top**[2], **Kristina B. Kooiker**[3,4,5,6], **Saffie Mohran**[3,6,7], **Christian Mandrycky**[3,7], **Tim McMillen**[3,6,7], **Michael Regnier**[3,4,6,7], **Thomas C. Irving**[8,9], **Weikang Ma**[8,9], **Bertrand C.W. Tanner**[2]

[1]School of Molecular Biosciences, Washington State University, Pullman, Washington

[2]Department of Integrative Physiology and Neuroscience, Washington State University, Pullman, Washington

[3]Division of Cardiology, Department of Medicine, University of Washington, Seattle, Washington

[4]Center for Translational Muscle Research, University of Washington, Seattle, Washington

[5]Center for Cardiovascular Biology, University of Washington, Seattle, Washington

[6]Institute for Stem Cell and Regenerative Medicine, University of Washington, Seattle, Washington

[7]Department of Bioengineering, University of Washington, Seattle, Washington

[8]Department of Biology, Illinois Institute of Technology, Chicago, Illinois

[9]Center for Synchrotron Radiation Research and Instrumentation, Illinois Institute of Technology, Chicago, Illinois

Abstract

Precise regulation of sarcomeric contraction is essential for normal cardiac function. The heart must generate sufficient force to pump blood throughout the body, but either inadequate or excessive force can lead to dysregulation and disease. Myosin regulatory light chain (RLC) is a thick-filament protein that binds to the neck of the myosin heavy chain. Post-translational phosphorylation of RLC (RLC-P) by myosin light chain kinase is known to influence acto-myosin interactions, thereby increasing force production and Ca^{2+}-sensitivity of contraction. Here, we investigated the role of RLC-P on cardiac structure and function as sarcomere length and [Ca^{2+}] were altered. We found that at low, non-activating levels of Ca^{2+}, RLC-P contributed to myosin

*Address for Correspondence: Bertrand C.W. Tanner, Room 255 Vet/Biomed Research Building, 1815 Ferdinand's Lane, Department of Integrative Physiology and Neuroscience, Washington State University, Pullman, WA. 99164-7620, bertrand.tanner@wsu.edu, fax: (509)-335-4650.

Author contributions

KT and BCWT conceptualized the work. All authors contributed to the acquisition, analysis, and interpretation of the work. All authors contributed to revising the work, approve of the final document for publication, and agree to be accountable for all aspects of the work. All authors qualify for authorship, and all persons who qualify for authorship are listed as authors.

Competing interests

T.I and W.M provides consulting and collaborative research studies to Edgewise Therapeutics, but such work is unrelated to the content of this article.

head disorder, though there were no effects on isometric stress production and viscoelastic stiffness. With increases in sarcomere length and Ca^{2+}-activation, the structural changes due to RLC-P become greater, which translates into greater force production, greater viscoelastic stiffness, slowed myosin detachment rates, and altered nucleotide handling. Altogether, these data suggest that RLC-P may alter thick-filament structure by releasing ordered, off-state myosin. These more disordered myosin heads are available to bind actin, which could result in greater force production as Ca^{2+} levels increase. However, prolonged cross-bridge attachment duration due to slower ADP release could delay relaxation long enough to enable cross-bridge rebinding. Together, this work further elucidates the effects of RLC-P in regulating muscle function, thereby promoting a better understanding of thick-filament regulatory contributions to cardiac function in health and disease.

Graphical Abstract

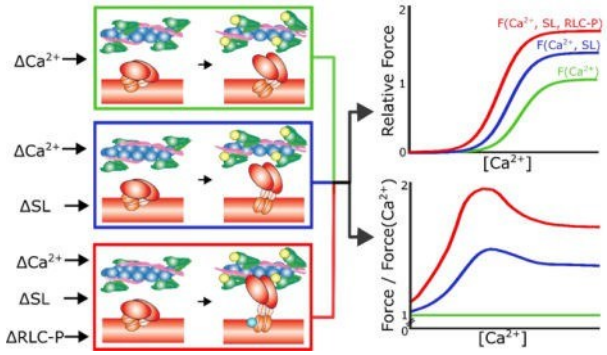

Increases in $[Ca^{2+}]$ (yellow circles), sarcomere length (SL), and phosphorylation of regulatory light chain (RLC-P; blue circle) all contribute to increases in myocardial contractility. We investigated the role of RLC-P on cardiac structure and function while $[Ca^{2+}]$ and SL were altered. Increasing $[Ca^{2+}]$, SL, and RLC-P increased disorder of the myosin heads along the thick-filament, which led to increased isometric stress, greater viscoelastic myocardial stiffness, and prolong cross-bridge attachment due to slowed ADP release from strongly bound myosin heads. These findings demonstrate a progressive pathway of myofilament activation whereby increases in RLC-P amplify force production due to increases in $[Ca^{2+}]$ and SL.

Introduction

Myosin regulatory light chain (RLC) is a thick-filament protein that binds to the myosin neck region. RLC can be post-translationally phosphorylated by the Ca^{2+}- and calmodulin dependent kinase, myosin light chain kinase (MLCK) to increase force production and calcium sensitivity (Pulcastro *et al*., 2016). RLC phosphorylation (RLC-P) plays a vital role in the sarcomere, where it is thought to regulate the interaction between myosin and actin filaments, with increases in RLC-P leading to greater contractility at the molecular and cellular levels. This translates into greater cardiac output and stroke volume at the organ level throughout each heartbeat (Scruggs *et al*., 2009; Scruggs & Solaro, 2011; Perike *et al*., 2023). The dynamic nature of RLC-P allows the heart to adapt to varying physiological demands, with increased phosphorylation optimizing contractile performance during periods

of heightened demand. Better understanding the effects of RLC-P on cardiac contractility is crucial for unraveling the complexities of cardiac physiology.

The Frank-Starling law of the heart describes an important physiological response that appears intrinsic to organ level function: as the volume of blood filling the ventricle increases, cardiac contractility increases—balancing ventricular stroke volume with venous return on a beat-to-beat basis (Shiels & White, 2008). At the cellular level, muscle force production and Ca^{2+}-sensitivity of contraction increase as sarcomere length (SL) increases, thereby defining an intrinsic mechanism of contractility called length-dependent activation that represents the primary mechanism underlying the Frank-Starling relationship (de Tombe *et al*., 2010; Campbell *et al*., 2018; Kosta & Dauby, 2021). Although the individual effects of regulatory proteins on length-dependent activation and contractile dynamics are starting to be elucidated, the role that RLC-P contributes to cardiac function as SL and Ca^{2+} levels change is not well-defined.

The coordinated regulation of RLC-P, SL, and Ca^{2+} is imperative for optimal cardiac function, as failure to maintain the proper impact of either process on myofilament function may result in cardiac dysfunction. RLC-P has emerged as a player in the pathogenesis of cardiovascular diseases (Toepfer *et al*., 2013), with dysregulated RLC-P altering contractile dynamics, impairing relaxation, and contributing to structural remodeling of the myocardium (Markandran *et al*., 2021, 2022). Ischemic heart disease and reperfusion injury can influence compensatory RLC phosphorylation dynamics, impacting contractile function and exacerbating tissue damage (Akiyama *et al*., 1997). This study aimed to improve our understanding of the effects of RLC phosphorylation on myofilament structure and function in β-myosin expressing porcine cardiac tissue, which is more translatable to human health and disease compared to prior biophysical studies that have primarily used α-myosin expressing rodent cardiac tissue. Understanding the nuanced roles of RLC-P in heath and disease mechanisms will help unravel and identify potential therapeutic targets for normalizing pathophysiological muscle regulation.

Materials and Methods

Porcine Tissue

Two porcine hearts from 3-month-old male pigs were purchased from Exemplar Genetics (Sioux Center, IA, USA). The tissues were obtained in compliance with protocols approved by the Institutional Animal Care and Use Committees of the respective institutes and no live animals were involved in this study. Thus, no institutional approval is required by Washington State University. Solely using male porcine cardiac tissue in this study limits our capacity to extend our novel findings concerning the effects of RLC-P on cardiac function as SL and [Ca^{2+}] varied to both sexes.

Solutions

Solution recipes were calculated and prepared as outlined by Godt & Lindley (1982). All values are in mM unless otherwise specified. Relaxing solution: pCa 8.0 (pCa = $-\log_{10}[Ca^{2+}]$), 5 EGTA, 5 MgATP, 1 Mg^{2+}, 0.3 Pi, 35 phosphocreatine, 300 U/mL creatine

kinase (CK), 200 ionic strength, 3% dextran T-500 (wt/vol), pH 7.0. Activating solution was the same as relaxing solution but adjusted to a free [Ca^{2+}] of pCa 4.8. Dissecting solution: 50 BES, 30.83 K propionate, 10 Na azide, 20 EGTA, 6.29 MgCl2, 6.09 ATP, 1 DTT, 20 BDM, 50 Leupeptin, 275 Pefabloc, and 1 E-64. Permeabilizing (skinning) solution: Dissecting solution with 1% Triton X-100 (vol/vol) and 50% glycerol wt/vol. Storage solution: Dissecting solution with 50% glycerol (vol/vol). Alkaline phosphatase (AP) solution: relaxing solution with 170 U/mL AP (sc-3716, ChemCruz). Myosin light chain kinase (MLCK) solution: relaxing solution, but adjusted to pCa 6.25, 1.1 μM human skeletal MLCK, and 12 μM *Xenopus* calmodulin. MLCK sham solution: relaxing solution, adjusted to pCa 6.25 and 12 μM *Xenopus* calmodulin.

X-ray Diffraction

X-ray diffraction experiments were performed at the BioCAT beamline 18ID at the Advanced Photon Source, Argonne National Laboratory (Fischetti *et al*., 2004). The x-ray beam wavelength was set to 0.1033 nm (12 KeV) and the incident beam flux was attenuate to ~5 $\times 10^{12}$ photons per second. Skinned porcine myocardial strips were stretched to a sarcomere length of 1.9 or 2.2 μm by monitoring light diffraction patterns from a helium-neon laser (633 nm). X-ray fiber diffraction patterns were collected at 1.9 μm SL in pCa 8.0 solution after incubation with AP or MLCK, stretched to 2.2 μm, and then sub-maximally activated to pCa 5.6 at room temperature (~23°C). Resulting x-ray diffraction patterns were analyzed using the MuscleX software package developed at BioCAT (Jiratrakanvong *et al*., 2018). The equatorial reflections were analyzed by the Equator module in the MuscleX software package as detailed previously (Ma & Irving, 2022). X-ray patterns were subsequently quadrant folded and background subtracted to improve signal to noise ratio for further analysis using the Quadrant Fold module of the MuscleX program suite. The meridional and layer line reflections were measured using the Projection Traces module of MuscleX program suite as described previously (Ma *et al*., 2018, 2020). The measured intensities of x-ray reflections are normalized to the sixth-order actin-based layer line intensities as described previously (Ma *et al*., 2022) to compare the intensities under different conditions. Three patterns per fiber were collected under each condition and the x-ray reflection data extracted from these patterns were averaged.

Muscle Mechanics

Tissue preparation: Frozen porcine left ventricle sections were placed in a vial with dissecting solution and left on ice for ~10 min to thaw. Tissue was transferred to a dish containing skinning solution, trimmed, and skinned overnight at 4°C. Skinned myocardial muscle preparations were transferred to storage solution, and if not used immediately for mechanics experiments, stored at −20° C for up to one week.

In all mechanical experiments, permeabilized left ventricular papillary muscles were dissected to approximately 180 μm in diameter and 700 μm in length. Aluminum T-clips were affixed to the end of each strip, and subsequently all strips underwent a 10-minute pre-treatment in an AP solution at room temperature. The strips were then positioned between a piezoelectric motor (P841.40, Physik Instrumente, Auburn, MA) and a strain gauge (AE801, Kronex, Walnut Creek, CA). The mounted strips were then immersed in a 30 μL droplet of

relaxing solution, maintained at 23°C, and stretched to a sarcomere length of 1.9 μm or 2.2 μm, measured by digital Fourier Transform routine (IonOptix Corp, Milton, MA).

Muscle strips were then either incubated in MLCK solution or MLCK sham solution for 60 minutes. Strips were relaxed to pCa 8.0, and then activated with Ca^{2+}, transitioning from pCa 8.0 to sub-maximal [Ca^{2+}], and then to pCa 4.8. Isometric steady-state stress (=force per cross-sectional area) was recorded. At least 3 strips from each heart were used per condition. AP treatment reduced RLC-P from 24±1% (=No treatment, dashed line in Fig. 1) to 17±3%, providing a non-significant but consistent, basal level of RLC phosphorylation prior to MLCK treatment. MLCK treatment increased RLC-P to 70±3% but did not affect cardiac troponin I or cardiac myosin binding protein-C phosphorylation levels (Fig. 1). Relative levels of phosphorylation were quantified using GelBox (Gulbulak et al., 2024) to measure protein density from SYPRO Ruby total protein stain and Pro-Q Diamond phosphoprotein stain after mechanics experiments were performed.

Viscoelastic stiffness: Sinusoidal length perturbations of 0.125% myocardial strip length (clip-to-clip) were applied at multiple discreet frequencies from 0.8 to 100 Hz to measure the complex modulus as a function of frequency (Kawai & Brandt, 1980; Mulieri *et al*., 2002; Palmer *et al*., 2007). The complex modulus represents viscoelastic myocardial stiffness, which arises from the change in stress divided by the change in muscle length that is in-phase (elastic modulus) and out-of-phase (viscous modulus) with the oscillatory length change at each frequency.

Characteristics of the elastic and viscous moduli responses over the measured frequency range provide a signature of cross-bridge binding and cycling kinetics. These data were fit to Eq. 1 to extract the 6 parameters describing viscoelastic tissue response as a function of angular frequency (ω):

$$Y(\omega) = A(i\omega)^k - B\left(\frac{i\omega}{2\pi b + i\omega}\right) + C\left(\frac{i\omega}{2\pi c + i\omega}\right)$$

Eq. (1)

The complex modulus, Y(ω), originates from the passive structural elements within the muscle and the force-generating cross-bridges. The A-process arises from passive mechanical elements within the tissue. The parameter A encapsulates the combined mechanical stiffness of the filaments and the number of strongly bound cross-bridges, while k characterizes the viscoelastic response's nature where k = 0 is entirely elastic and k = 1 is entirely viscous. The B- and C-processes signify enzymatic cross-bridge behavior in activated muscle, where B and C provide a metric of cross-bridge binding and their characteristic frequencies, 2πb and 2πc, provide a metric of cross-bridge attachment and detachment rate, respectively.

Nucleotide handling rates: Stress responses were recorded following a step-length change of 0.5% muscle length to assess cross-bridge kinetics as a function of [MgATP]. The stress response was fit to a dual exponential function to characterize the rate of stress release (k_{rel}) associated with the cross-bridge detachment rate as [MgATP] varied. Assuming

that strongly bound cross-bridge attachment events primarily occupy the myosin-MgADP and rigor states of the cross-bridge cycle as [MgATP] was titrated from 5 mM towards 0 mM, Eq. 2 can be used to describe k_{rel} as a function of [MgATP]. As [MgATP] decreases, cross-bridge detachment slows due to slower MgATP binding, which increases the amount of time a cross-bridge spends in the rigor state.

$$k_{rel}\left(MgATP \right) = \frac{k_{-ADP}[MgATP]}{\frac{k_{-ADP}}{k_{+ATP}} + [MgATP]} \quad \text{Eq. (2)}$$

The k_{rel} vs. MgATP relationship from each individual myocardial strip was fit to Eq. 2 to estimate the cross-bridge rates of MgADP release (k_{-ADP}) and MgATP binding (k_{+ATP}). The ratio of k_{-ADP}/k_{+ATP} represents the [MgATP] at half-maximal detachment rate, $[MgATP]_{50}$.

Statistical Analysis

All statistical analyses were performed using SPSS (IBM Statistics, Chicago, IL). Student's two-tailed, unpaired t-test was performed on data from Fig. 1 to determine changes in myofilament protein phosphorylation. Nested linear mixed models incorporating either two (Treatment, SL for Figs. 2 and 7–9) or three main effects (Treatment, SL, pCa for Figs. 3 and 4; or Treatment, SL, Frequency for Figs. 5 and 6) and their interactions were utilized for the x-ray diffraction parameters, stress responses, nucleotide handling rates, viscoelastic stiffness, and subsequent parameters. Nested linear mixed model analyses link data from the same hearts, with hearts being a random effect, to optimize statistical power. Post hoc analyses were performed where the main effects show a significant interaction using Fisher's least significant difference test, where p-values less than 0.05 were considered significant. Post-hoc p-values are indicated in the figure panels.

Results

Ca^{2+}-activated stress

At low $[Ca^{2+}]$ (pCa 8.0), steady-state isometric stress was not affected by MLCK treatment, but stress increased as SL increased (Fig. 2A). We measured Ca^{2+}-activated stress at two submaximal $[Ca^{2+}]$: pCa 5.6 and the $[Ca^{2+}]$ that produced half-maximal stress (i.e. ~pCa_{50}). Sub-maximal Ca^{2+}-activated stress values increased with MLCK treatment and SL (Fig. 2B and 2C) and increases in stress due to MLCK treatment appear to be amplified at longer SL ($p=0.007$ and $p=0.022$ for Treatment*SL interactions at pCa 5.6 and ½ maximal activation, respectively). Maximal Ca^{2+}-activated stress also increased with MLCK treatment and SL (Fig. 2D). Thus, increases in RLC-P due to MLCK treatment increased force production more at longer SL, and the relative increase in force production due to RLC-P was larger at submaximal $[Ca^{2+}]$.

X-ray diffraction

Small angle x-ray diffraction measurements characterize structural organization (or order) of the myosin heads, thick-filaments, and thin-filaments within permeabilized myocardial strips. The $d_{1,0}$ parameter represents thick-to-thick filament spacing (i.e., distance between the center of adjacent thick-filaments) within the myofilament lattice. We found that $d_{1,0}$ was not affected by MLCK treatment at low calcium (pCa 8.0, Fig. 3C), and that $d_{1,0}$ decreased as SL increased, indicating myofilament lattice compression that most likely stems from an increase in the radial component of titin-based passive force as the tissue is stretched (Linke, 2000; Linke & Fernandez, 2002; Fukuda *et al*., 2005; Irving *et al*., 2011; Ait-Mou *et al*., 2017). The parameter $d_{1,0}$ also increased when [Ca^{2+}] increased from pCa 8.0 to pCa 5.6, suggesting that: i) cross-bridge binding may expand the myofilament lattice (Williams *et al*., 2010), or ii) increases in isometric stress may be associated with internal shortening of the myocardial strip that decreases sarcomere length (Kawakami & Lieber, 2000; Caremani *et al*., 2019).

The equatorial intensity ratio, $I_{1,1}/I_{1,0,}$ depends on the relative amount of mass associated with the thick-filament backbone and the thin-filament; increases in $I_{1,1}/I_{1,0}$ indicate closer proximity of the myosin heads and the thin-filament (Ma & Irving, 2022). At low [Ca^{2+}], $I_{1,1}/I_{1,0}$ values were not affected by MLCK treatment, nor increases in SL (Fig. 3D). However, the addition of calcium (to pCa 5.6 at 2.2 μm SL) increased $I_{1,1}/I_{1,0}$ in both AP and MLCK treated strips. This indicates that increased [Ca^{2+}] facilitates myosin head movement toward the thin-filament, closer to actin-binding sites, as one might expect with the increase in isometric stress from pCa 8.0 to 5.6 (Fig. 2A, B).

Changes in the intensities and spacings of the meridional reflections are associated with order-to-disorder (i.e. OFF-to-ON) transitions along the length of the thick-filaments (Ma *et al*., 2023). The intensity of the 3rd order myosin meridional reflection (I_{M3}) arises from the 14.3 nm repeats of myosin crowns where the heads extend from the thick-filament backbone. MLCK treatment only decreased I_{M3} at 1.9 μm SL (pCa 8.0). I_{M3} also decreased as SL increased at pCa 8.0, and as [Ca^{2+}] increased (Fig. 4A). This indicates that MLCK treatment, increases in SL, and increases in Ca^{2+} all contribute to disordering the myosin heads.

The spacing of the 3rd myosin meridional reflection (S_{M3}) corresponds to the axial distance between the myosin crowns. MLCK treatment decreased S_{M3} at pCa 8.0 at both sarcomere lengths (Fig. 4B). However, MLCK treatment increased S_{M3} at pCa 5.6, which likely stems from longitudinal stretching of the thick-filaments due to increases in cross-bridge binding and force production at sub-maximal activation.

The intensity of the 6th order myosin meridional reflection (I_{M6}) arises from the 7.15 nm repeat of structures within the thick-filament backbone (Ma & Irving, 2022). Currently, there are no straightforward interpretations of changes in I_{M6}, except that the intensity decreases with increases in overall lattice organization or order. MLCK treatment decreased I_{M6} under all conditions (Fig. 4C), consistent with RLC-P disturbing the OFF state of myosin (Kampourakis *et al*., 2018). Increasing pCa from 8.0 to 5.6 also decreased I_{M6}, as expected with Ca^{2+}-activation of contraction. The spacing of the 6th order myosin meridional

reflection (S_{M6}) increased with MLCK treatment for both SLs at low [Ca^{2+}] (Fig. 4D). S_{M6} also showed consistent increases with SL and with sub-maximal Ca^{2+}-activation. Together, findings from the 6th order meridional intensity and spacing data suggest that structural changes along the thick-filament arise from increased strain along the filament backbone as force increases with SL and [Ca^{2+}].

Viscoelasticity at passive, sub-maximal, and maximal conditions

Sinusoidal length-perturbations were utilized to assess myocardial viscoelasticity at passive (pCa 8.0), sub-maximal (pCa 5.6 and half-maximal activation), and maximal Ca^{2+}-activation (pCa 4.8) conditions. At pCa 8.0 there were subtle, albeit consistent, increases in myocardial viscoelasticity with MLCK treatment, increases in SL, and increases in frequency ($p<0.001$ for main effect of Treatment, SL, and Frequency for elastic and viscous moduli vs. frequency relationships; Fig. 5). However, the greatest increases in elastic and viscous moduli followed from increases in SL at higher frequencies, for AP and MLCK treated strips. Thus, these increases in stiffness mirror the increases in passive tension with SL (Fig. 2A), suggesting greater stretching of the passive elements in the sarcomere, such as titin and collagen, as length increases.

Myocardial elasticity increased with MLCK treatment, increases in SL, and increases in frequency ($p<0.001$ for main effect of each for elastic moduli vs. frequency relationships; Fig. 6) for all Ca^{2+}-activated conditions. Again, this is consistent with the increases in isometric stress (Fig. 2). At pCa 5.6 and at half-maximal activation, the greatest, most consistent increases in elastic moduli occurred with MLCK treatment and longer SL (Fig. 6A, left and middle panels). At maximal Ca^{2+}-activation (pCa 4.8), MLCK treatment only increased elastic moduli over a narrow range of frequencies at 1.9 μm SL (Fig. 6A, right). These increases in elastic moduli reflect greater cross-bridge binding, and thus, MLCK treatment appears to have its largest effects on cross-bridge binding at sub-maximal calcium levels at longer SL.

Generally, changes in viscous moduli reflected the increases in elastic moduli described above. Shifts in the viscous moduli represent changes in the work-producing and work-absorbing characteristics of myocardium due to kinetic changes in cross-bridge cycling. At pCa 5.6 and half-maximal activation, viscous moduli increased with MLCK treatment and longer SL (Fig. 6B, left and middle). At maximal Ca^{2+}-activation (pCa 4.8), MLCK treatment only increased viscous moduli at 1.9 μm; viscous moduli also increased at longer SL for both treatment groups (Fig. 6B, right). Again, these viscous moduli vs. frequency data suggest that MLCK treatment has its greatest effect on cross-bridge activity at sub-maximal calcium levels.

Elastic and viscous moduli data from Fig. 6 were fit to Eq. 1 to extract six parameters describing cross-bridge function. The A parameter describes viscoelastic stiffness from passive elements (titin, collagen, and long-lived, strongly-bound cross-bridges) of the myocardium. At pCa 5.6 and half-maximal activation, both MLCK treatment and longer SL contributed to increases in A (Fig. 7A, left and middle). However, at maximal Ca^{2+}-activated conditions (pCa 4.8), A only increased longer SL (Fig. 7A, right). The parameter k is also involved in the A-process and indicates the degree of viscoelasticity in a system. If k were to

equal 0, this would represent a completely elastic system and if k were to equal 1, this would represent a completely viscous system. We observed no effects of MLCK treatment on k at pCa 5.6, half-maximal activation, or pCa 4.8 (Fig. 7B). Increasing SL decreased k, but only at half-maximal activation. Combined with x-ray diffraction results, these findings suggest that MLCK treatment increases viscoelastic stiffness because more cross-bridges can bind actin upon Ca^{2+}-activation, which could make the myofilament lattice appear stiffer. This also suggests that increases in sarcomere length likely stretch the passive elements of the sarcomere, such as titin and collagen, to increase elasticity of the myocardium (Linke & Fernandez, 2002; Irving *et al*., 2011).

The B- and C- processes arise from enzymatic cross-bridge activity. At sub-maximal calcium levels, MLCK treatment increased B, but only at longer SL (Fig. 8A left and middle). At maximal Ca^{2+}-activation, MLCK treatment increased B at short SL (1.9 μm). However, increasing SL from 1.9 μm to 2.2 μm increased B, but only for the AP treated group (Fig. 8A right). Similar trends were also observed in parameter C (Fig. 8B). Taken together, these findings are consistent with the x-ray, force, and sinusoidal analysis data further suggesting that MLCK treatment augments Ca^{2+}-activated cross-bridge binding. There are, however, some divergent results with Ca^{2+}-activation, showing that effects of MLCK treatment on cross-bridge binding occur primarily at 1.9 μm SL with maximal Ca^{2+}-activation (pCa 4.8). Albeit consistent with prior findings, the effects of MLCK on cross-bridge binding are greater at longer SL during sub-maximal Ca^{2+}-activation levels, which may be more important to physiological contraction (which occurs at sub-maximal $[Ca^{2+}]$).

The parameter 2πb is a measure of cross-bridge attachment rate stemming from the B process (Pulcastro *et al*., 2016; Breithaupt *et al*., 2019; Awinda *et al*., 2020). We did not observe any significant changes in attachment rate associated with MLCK treatment, SL, or Ca^{2+} levels (Fig.8C). The parameter 2πc is a measure of cross-bridge detachment rate stemming from the C process. MLCK treatment decreased 2πc at all three $[Ca^{2+}]$ at 1.9 μm SL (Fig. 8F). To summarize these kinetic measurements, we show that cross-bridge detachment rate slowed with RLC-P, but only at the short sarcomere length (for all three Ca^{2+}-activation levels).

Nucleotide handling rates

Nucleotide handling rates were assessed using a step-stretch protocol, where tissue preparations were stretched by 0.5% of total muscle length and the stress response was recorded as [ATP] varied (Fig. 9). The raw stress vs. time responses were fit to a double exponential equation to extract the parameter k_{rel}, a measure of cross-bridge release rate (Fig. 9A; lower panel). When k_{rel} was plotted against [ATP], we observed that both MLCK treatment and longer SL decreased k_{rel} (Fig. 9B).

Individual k_{rel} vs. [ATP] relationships were fit to Eq. 2 to extract the nucleotide handling rates k_{-ADP}, k_{+ATP}, and the ATP concentration yielding half-maximal dissociation, $[MgATP]_{50}$. The rate of ADP release, k_{-ADP}, decreased with MLCK treatment at both SL (Fig. 9C). Conversely, the rate of ATP association, k_{+ATP}, increased with MLCK treatment at both SL (Fig. 9D). The [MgATP] concentration at half-maximal detachment

rate, $[MgATP]_{50}$, also decreased with MLCK treatment, and the effect of MLCK treatment was greater at the shorter SL (Fig. 9E). These data indicate that MLCK treatment slows ADP release, which may be contributing to greater Ca^{2+}-activated stress values (Fig. 2D). Slower ADP release could also prolong cross-bridge attachment duration via slower myosin detachment to augment force, given that ADP release is the rate limiting step of the cross-bridge cycle in a muscle fiber (Siemankowski *et al*., 1985).

Discussion

We analyzed the effects of RLC phosphorylation (RLC-P) on myocardial structure and function in permeabilized myocardial strips from the porcine left ventricle at two sarcomere lengths, and at multiple Ca^{2+}-activation levels. Experimental data included x-ray diffraction, isometric muscle mechanics, and cross-bridge kinetics measurements while RLC-P levels were modulated via alkaline phosphatase (AP) or myosin light chain kinase (MLCK) treatment. In summary, we found that MLCK treatment causes an increase in the disorder of myosin heads resulting in more heads available to bind actin, more force production, greater viscoelastic myocardial stiffness, and prolonged cross-bridge binding as SL and $[Ca^{2+}]$ increased—demonstrating a pathway for progressive activation of the myocardium.

At low $[Ca^{2+}]$ (pCa 8.0), we found that MLCK treatment alone did not alter the equatorial x-ray diffraction parameters $d_{1,0}$ (=myofilament lattice compression), and $I_{1,1}/I_{1,0}$ (=myosin heads moving towards the thin-filament), indicating that RLC-P did not affect lattice spacing nor movement of myosin heads away from the thick-filament backbone toward the thin-filament (Fig. 3C–D). In agreement with these structural data, functional measurements showed that MLCK treatment did not affect isometric stress nor viscoelastic myocardial stiffness at low $[Ca^{2+}]$ (Fig. 2A & 5). Comparable measurements from a previous study that used permeabilized mouse myocardial strips showed that RLC-P decreased $d_{1,0}$ and increased $I_{1,1}/I_{1,0}$ (Colson *et al*., 2010). These structural changes correlated with an increase in passive force (pCa 9.0) with MLCK treatment. In addition to the differences in species, this prior study was performed at room temperature, under relaxed conditions (pCa 9.0), with no dextran at 2.15 μm SL. Our study herein used porcine myocardium, also at room temperature, but we made measurements over multiple $[Ca^{2+}]$ and different sarcomere lengths (1.9 and 2.2 μm), with all of our solutions having 3% dextran (w/vol); the latter of which osmotically-compresses the myofilament lattice to better emulate physiological lattice spacing in intact muscle preparations (Tanner *et al*., 2012; Miller *et al*., 2015; Kawai & Schulman, 1985; Irving *et al*., 2011). Thus, it is plausible that the reduction in myofilament lattice spacing due to dextran has a greater influence on equatorial x-ray diffraction parameters than RLC-P at low $[Ca^{2+}]$.

Consistent with this idea, and our passive mechanics data, Yang *et al*., 1998 showed that RLC-P did not affect isometric force at low $[Ca^{2+}]$ in the presence of 4–8% dextran using skinned rabbit psoas preparations, but RLC-P increased passive tension in the absence of dextran (Yang *et al*., 1998). We have not observed any effects of RLC-P on isometric tension at low $[Ca^{2+}]$ in the presence or absence of dextran using permeabilized myocardial strips from mice or rats (Pulcastro *et al*., 2016; Breithaupt *et al*., 2019; Turner *et al*., 2023). There is more tissue from the porcine heart, compared to rodents, which enables

larger myocardial preparations for the x-ray diffraction measurements. These larger tissue preparations typically increase the intensity and quality of the x-ray diffraction patterns, compared to permeabilized myocardial strips from mice or rats. Therefore, the attenuated effects of RLC-P on equatorial diffraction parameters that we see in our measurements (Fig. 3) compared to comparable measurement from Colson *et al. 2010* could stem from multiple differences in experimental design between the two studies. Nonetheless, it is likely that our observations more closely describe structural and accompanying mechanical responses to RLC-P under near-physiological conditions (with osmotic compression) than previous studies.

At low [Ca^{2+}] we also found that MLCK treatment mostly affected the meridional x-ray reflections, with RLC-P decreasing I_{M3}, S_{M3}, and I_{M6} and increasing S_{M6} at both SLs. The consensus in the field has been that I_{M3} comes primarily from the myosin heads while the intensity of the 6th order meridional reflections, I_{M6}, arises primarily from structures within the myofilament backbone, including titin and myosin binding protein C. In support of this notion, time resolved intensity data show different time course for the spacings and intensities of the M3 and M6 reflections indicating that they are reporting different underlying structures (Ma *et al*., 2020). However, recent cryo-electron microscopy analyses of the C-zone in the presence of mavacamten indicate, at least under these conditions, that there can be a substantial contribution of myosin heads to the M6 intensity ($I_{M6,}$ Ma & Irving, 2022; Dutta *et al*., 2023). While the possibility that I_{M6} data may reflect structural changes in myosin head orientations, and/or other structural changes cannot be excluded, a more likely explanation for the observed reduction in I_{M6} with MLCK treatment (Fig. 4) is that increased RLC-P simply decreases overall thick-filament order. A better definition of structures that contribute to these higher-order meridional reflections is required for a more detailed interpretation of the influence of MLCK treatment on thick-filament structure. As discussed above, we did not observe any differences in isometric stress or viscoelastic stiffness due to MLCK treatment at pCa 8.0, despite indications of increased disorder of the myosin heads. Interactions between the thick- and thin- filament are predominantly calcium-dependent and are mediated by regulatory proteins troponin and tropomyosin (Moore *et al*., 2016). Therefore, regardless of RLC-P, inhibitory effects of the thin-filament prevent cross-bridge binding and force production at low [Ca^{2+}]. Others have also shown that increases in RLC-P induce myosin head disorder (Alamo *et al*., 2015; Kampourakis & Irving, 2015; Kampourakis *et al*., 2016). Together, these data indicate that increasing RLC-P may have subtle effects on myocardial structure at low [Ca^{2+}] that do not affect isometric stress or stiffness in our measurements.

Unlike MLCK treatment, increasing SL at low [Ca^{2+}] resulted in multiple structural and functional changes. Increasing SL from 1.9 μm to 2.2 μm: i) reduced lattice spacing (=decreased $d_{1,0}$, Fig. 3A), as was expected (de Beer *et al*., 1988; Fuchs & Wang, 1996; Irving *et al*., 2000); ii) increased myosin head disorder (=decreased I_{M3} and I_{M6}; Fig. 3C,E); and iii) increased thick-filament backbone stretch (=increased S_{M6}; Fig. 3F), likely due to increased thick-filament strain when stretching the sarcomere. These SL-dependent structural changes were coupled with increases in stress and viscoelastic myocardial stiffness (Fig 3A, B). Many of these responses were anticipated, given our prior studies showing that increases in SL contribute to myosin head movement off the

thick-filament backbone toward the thin-filament, increase passive force production, and increases myocardial stiffness (Breithaupt *et al*., 2019; Awinda *et al*., 2020; Ma *et al*., 2021). Thus, the largest effects on myocardial structure and function that we observed at pCa 8.0 arose from increasing SL, not changes in RLC-P.

Effects of MLCK treatment and increasing SL on myocardial structure and function were amplified upon Ca^{2+} activation. Below we first discuss the structural responses to increasing [Ca^{2+}] that we observed, and next the mechanical responses to increasing [Ca^{2+}]. Increasing [Ca^{2+}] from pCa 8.0 to pCa 5.6 increased lattice spacing (=increased $d_{1,0}$; Fig 3C), which we found intriguing, and may support recent theories that myosin heads work to decompress the lattice when bound. Ca^{2+}-activation further decreased myosin head order and spacing along the thick-filament (=decreased I_{M3} and increased S_{M6}; Fig 4A, D). These responses could follow from increased force production at pCa 5.6 activating mechanosensitive thick-filament regulatory mechanisms to augment the population of cross-bridges available to bind with actin (de Tombe *et al*., 2010; Brunello *et al*., 2023). As with our observations at pCa 8.0, MLCK treatment did not alter any equatorial diffraction parameters ($d_{1,0}$ and $I_{1,1}/I_{1,0}$; Fig. 3C–D) at pCa 5.6. One prior study suggested that RLC-P independently alters myosin head conformation to a pre-defined conformation, rather than simply disordering the heads (Kampourakis & Irving, 2015). Kampourakis & Irving proposed that RLC-P modulates contractility via a more complex mechanism than only movement of myosin heads towards the thin-filament, in agreement with our observations.

We also observed subtle, but consistent, increases in $I_{1,1}/I_{1,0}$ as SL and Ca^{2+} increased, suggesting that both SL and [Ca^{2+}] increase the probability of cross-bridge binding due to the increased proximity of the myosin heads to actin. This could augment mechanosensitive recruitment of myosin heads from the OFF population toward the ON population and concomitantly amplify cooperative cross-bridge contributions to thin-filament activation (Moore *et al*., 2016; Ma *et al*., 2023). This highlights the dual-filament regulatory pathways that have been under intense investigation over the past decade, which could cooperatively amplify cross-bridge binding and force production (Brunello *et al*., 2023). Moreover, these coupled thick- and thin-filament regulatory pathways could also enhance relaxation during cooperative de-activation of both filaments as [Ca^{2+}] and force decrease during diastole (Brunello & Fusi, 2024).

It was interesting that MLCK treatment did not increase $I_{1,1}/I_{1,0}$ values at any single pCa or SL value ($p = 0.335$ for the fixed effect of treatment, Fig. 3D). However, we see a clear effect of increasing SL and pCa, both of which independently increase $I_{1,1}/I_{1,0}$ ($p = 0.023$ for the fixed effect of SL and $p < 0.001$ for the fixed effect of pCa, Fig. 3D). Increases in SL and pCa may have a greater effect on $I_{1,1}/I_{1,0}$ than MLCK, thereby masking any anticipated increases in $I_{1,1}/I_{1,0}$ from MLCK treatment. Our findings suggest this may be isolated to the $I_{1,1}/I_{1,0}$ measurement, given other data indicating that MLCK treatment augments the myosin ON transition (Fig. 4) to increase the population of strongly bound cross-bridges (Fig. 6 and Fig. 8A–B) and force production (Fig. 2) at sub-maximal or maximal calcium concentrations. It is plausible that the relative effect of [Ca^{2+}] or RLC-P on increased $I_{1,1}/I_{1,0}$ values are amplified in the presence of activating [Ca^{2+}] at the longer SL.

As [Ca^{2+}] increased from pCa 8.0, MLCK treatment increased isometric stress values (Fig. 2B–D), as well as myocardial viscoelastic stiffness (Fig. 6). This suggests that the effects of RLC-P are amplified with Ca^{2+}-activation of the myocardium, building on our prior observations that RLC-P increases Ca^{2+}-activated force production, and that this effect of RLC-P appears to be amplified with increases in SL (Pulcastro *et al*., 2016; Breithaupt *et al*., 2019; Turner *et al*., 2023). We also found that the A-parameter, extracted by fitting the viscoelastic myocardial stiffness data to Eq. 1, increased with RLC-P and SL (Fig. 7A). Increases in the A-parameter represent greater myocardial stiffness stemming from passive elements of the myocardium, such as titin, extracellular-matrix, and strongly bound cross-bridges that do not transiently attach nor detach throughout the oscillatory period of a single sinusoidal length-perturbation (at any single frequency). Thus, a portion of the increases in A could follow from more strongly bound cross bridges with MLCK treatment, which is amplified at longer SL. This agrees with our observations that MLCK treatment and increasing SL both increased S_{M6} (Fig 4D), which is an indicator of increased strain in the thick-filament backbone.

As Ca^{2+}-activation increased, MLCK treatment slowed ADP dissociation from myosin cross-bridges, as measured via step-perturbation analysis (Fig. 5C). These RLC-P dependent changes in nucleotide handling underly the slowed cross-bridge detachment rate (reduced $2\pi c$; Fig. 8D) given that ADP release is the rate limiting step of this cycle and slowing of ADP dissociation would correlate with increased cross-bridge binding duration (Siemankowski *et al*., 1985). Consistent with the observed changes in cross-bridge kinetics with sinusoidal analysis (Figs. 6–8), we see that increasing SL also slows (albeit qualitatively, not statistically significant) ADP release as we had previously observed (Pulcastro *et al*., 2016; Breithaupt *et al*., 2019). MLCK treatment also increased ATP binding rates and myosin affinity for ATP ($MgATP_{50}$; Fig. 9D–E). These changes in nucleotide handling rates could arise from RLC-P causing a conformational change in the lever arm, corresponding to altered positioning of the myosin head and subsequent altered binding affinities for ADP and ATP that facilitates greater cross-bridge binding with RLC-P that is augmented by increases in SL.

Altogether these data show that increases in RLC-P and SL cause structural changes in myofilament organization under relaxed (pCa 8.0) conditions that are primarily associated with altered meridional reflections (i.e. I_{M6}, S_{M6}). These structural changes under relaxed conditions persist at sub-maximal and maximal Ca^{2+}-activation levels, leading to functional changes in myofilament mechanics, namely increases in isometric stress, viscoelastic stiffness, and prolonged cross-bridge attachment due to slowed ADP release. These findings demonstrate a progressive pathway of activation wherein RLC-P, SL, and [Ca^{2+}] collectively contribute to increases in myofilament activation, which augment cross-bridge binding and force production. Reductions in RLC-P are often associated with the progression of heart disease, or end stage heart failure—compared to “normal” tissue. Thus, constitutive RLC-P is being explored as a potential therapy to ameliorate the progression of heart disease. Recent studies utilizing phosphomimetic animal models that mimic constitutive RLC-P have demonstrated cardioprotective effects of RLC-P in instances of *MYL2* mutations and restrictive and dilated cardiomyopathies (Warren *et al*., 2012; Yadav & Szczesna-Cordary, 2017; Kazmierczak *et al*., 2023; Liang *et al*., 2024). Better understanding of the role RLC-P

plays in heath and disease is imperative to its potential development as a therapeutic target to maintain adequate cardiac function and benefit patients with heart disease. Herein, we demonstrate that RLC-P, in combination with other myofilament mechanisms, is critical for fine tuning myofilament function.

Data availability statement

All data supporting the results of the study are available within the published paper. Any additional information is available from the authors upon request.

Funding

This work was supported by grants from the American Heart Association (23TPA1074093 https://doi.org/10.58275/AHA.23TPA1074093.pc.gr.172307 to BCWT), National Science Foundation (2312925 to BCWT), National Institutes of Health (R01HL149164 to BCWT, 1R01HL171657 to WM, HL128368 to MR, GM131981 to MR), and National Institute of Arthritis and Musculoskeletal and Skin Diseases (P30 AR074990 to MR). This research used resources of the Advanced Photon Source, a U.S. Department of Energy (DOE) Office of Science User Facility operated for the DOE Office of Science by Argonne National Laboratory under Contract No. DE-AC02-06CH11357. BioCAT is supported by grant P30 GM138395 from the National Institute of General Medical Sciences of the National Institutes of Health. The content is solely the authors' responsibility and does not necessarily reflect the official views of the National Institutes of Health.

Biography

Kyrah L. Turner received her BS in Biochemistry at Washington State University, where she is now a PhD Candidate studying in the laboratory of Dr. Bertrand C.W. Tanner. The focus of her PhD research is teasing apart thick-filament regulatory interactions in the cardiac sarcomere. She integrates biochemical and biophysical approaches to probe how post-translational modifications (such as phosphorylation) alter cross-bridge function and contractile dynamics of the myocardium. She plans to continue her training in cardiac physiology as a post-doctoral fellow, and later, as a faculty member studying cardiac biology in her own laboratory at a research-intensive university.

Works Cited

Ait-Mou Y, Zhang M, Martin JL, Greaser ML & de Tombe PP (2017). Impact of titin strain on the cardiac slow force response. Prog Biophys Mol Biol 130, 281–287.

Akiyama K, Akopian G, Jinadasa P, Gluckman TL, Terhakopian A, Massey B & Bing RJ (1997). Myocardial infarction and regulatory myosin light chain. J Mol Cell Cardiol 29, 2641–2652.

Alamo L, Li XE, Espinoza-Fonseca LM, Pinto A, Thomas DD, Lehman W & Padrón R (2015). Tarantula myosin free head regulatory light chain phosphorylation stiffens N-terminal extension, releasing it and blocking its docking back. Mol Biosyst 11, 2180–2189.

Awinda PO, Bishaw Y, Watanabe M, Guglin MA, Campbell KS & Tanner BCW (2020). Effects of mavacamten on Ca2+ sensitivity of contraction as sarcomere length varied in human myocardium. Br J Pharmacol 177, 5609–5621.

de Beer EL, Grundeman RL, Wilhelm AJ, van den Berg C, Caljouw CJ, Klepper D & Schiereck P (1988). Effect of sarcomere length and filament lattice spacing on force development in skinned cardiac and skeletal muscle preparations from the rabbit. Basic Res Cardiol 83, 410–423.

Breithaupt JJ, Pulcastro HC, Awinda PO, DeWitt DC & Tanner BCW (2019). Regulatory light chain phosphorylation augments length-dependent contraction in PTU-treated rats. J Gen Physiol 151, 66–76.

Brunello E & Fusi L (2024). Regulating Striated Muscle Contraction: Through Thick and Thin. Annu Rev Physiol 86, 255–275.

Brunello E, Marcucci L, Irving M & Fusi L (2023). Activation of skeletal muscle is controlled by a dual-filament mechano-sensing mechanism. Proceedings of the National Academy of Sciences 120, e2302837120.

Campbell KS, Janssen PML & Campbell SG (2018). Force-Dependent Recruitment from the Myosin Off State Contributes to Length-Dependent Activation. Biophys J 115, 543–553.

Caremani M, Brunello E, Linari M, Fusi L, Irving TC, Gore D, Piazzesi G, Irving M, Lombardi V & Reconditi M (2019). Low temperature traps myosin motors of mammalian muscle in a refractory state that prevents activation. J Gen Physiol 151, 1272–1286.

Colson BA, Locher MR, Bekyarova T, Patel JR, Fitzsimons DP, Irving TC & Moss RL (2010). Differential roles of regulatory light chain and myosin binding protein-C phosphorylations in the modulation of cardiac force development. J Physiol 588, 981–993.

Dutta D, Nguyen V, Campbell KS, Padrón R & Craig R (2023). Cryo-EM structure of the human cardiac myosin filament. Nature 623, 853–862.

Fischetti R, Stepanov S, Rosenbaum G, Barrea R, Black E, Gore D, Heurich R, Kondrashkina E, Kropf AJ, Wang S, Zhang K, Irving TC & Bunker GB (2004). The BioCAT undulator beamline 18ID: a facility for biological non-crystalline diffraction and X-ray absorption spectroscopy at the Advanced Photon Source. J Synchrotron Rad 11, 399–405.

Fuchs F & Wang YP (1996). Sarcomere length versus interfilament spacing as determinants of cardiac myofilament Ca2+ sensitivity and Ca2+ binding. J Mol Cell Cardiol 28, 1375–1383.

Fukuda N, Wu Y, Farman G, Irving TC & Granzier H (2005). Titin-based modulation of active tension and interfilament lattice spacing in skinned rat cardiac muscle. Pflugers Arch - Eur J Physiol 449, 449–457.

Godt RE & Lindley BD (1982). Influence of temperature upon contractile activation and isometric force production in mechanically skinned muscle fibers of the frog. J Gen Physiol 80, 279–297.

Gulbulak U, Wellette-Hunsucker AG & Campbell KS (2024). GELBOX: OPEN-SOURCE SOFTWARE TO IMPROVE RIGOR AND REPRODUCIBILITY WHEN ANALYZING GELS AND IMMUNOBLOTS. bioRxiv2024.03.07.583941.

Irving T, Wu Y, Bekyarova T, Farman GP, Fukuda N & Granzier H (2011). Thick-Filament Strain and Interfilament Spacing in Passive Muscle: Effect of Titin-Based Passive Tension. Biophysical Journal 100, 1499–1508.

Irving TC, Konhilas J, Perry D, Fischetti R & de Tombe PP (2000). Myofilament lattice spacing as a function of sarcomere length in isolated rat myocardium. Am J Physiol Heart Circ Physiol 279, H2568–2573.

Jiratrakanvong J, Shao J, Li X, Li J, Ma W, Agam G & Irving T (2018). MuscleX: software suite for diffraction X-ray imaging. Available at: doi:10.5281/zenodo.1195050.

Kampourakis T & Irving M (2015). Phosphorylation of myosin regulatory light chain controls myosin head conformation in cardiac muscle. J Mol Cell Cardiol 85, 199–206.

Kampourakis T, Ponnam S & Irving M (2018). Hypertrophic cardiomyopathy mutation R58Q in the myosin regulatory light chain perturbs thick filament-based regulation in cardiac muscle. Journal of Molecular and Cellular Cardiology 117, 72–81.

Kampourakis T, Sun Y-B & Irving M (2016). Myosin light chain phosphorylation enhances contraction of heart muscle via structural changes in both thick and thin filaments. Proceedings of the National Academy of Sciences 113, E3039–E3047.

Kawai M & Brandt PW (1980). Sinusoidal analysis: a high resolution method for correlating biochemical reactions with physiological processes in activated skeletal muscles of rabbit, frog and crayfish. J Muscle Res Cell Motil 1, 279–303.

Kawai M & Schulman MI (1985). Crossbridge kinetics in chemically skinned rabbit psoas fibres when the actin-myosin lattice spacing is altered by dextran T-500. J Muscle Res Cell Motil 6, 313–332.

Kawakami Y & Lieber RL (2000). Interaction between series compliance and sarcomere kinetics determines internal sarcomere shortening during fixed-end contraction. J Biomech 33, 1249–1255.

Kazmierczak K, Liang J, Maura LG, Scott NK & Szczesna-Cordary D (2023). Phosphorylation Mimetic of Myosin Regulatory Light Chain Mitigates Cardiomyopathy-Induced Myofilament Impairment in Mouse Models of RCM and DCM. Life (Basel) 13, 1463.

Kosta S & Dauby PC (2021). Frank-Starling mechanism, fluid responsiveness, and length-dependent activation: Unravelling the multiscale behaviors with an in silico analysis. PLoS Comput Biol 17, e1009469.

Liang J, Kazmierczak K, Veerasammy M, Yadav S, Takeuchi L, Kanashiro-Takeuchi R & Szczesna-Cordary D (2024). Mechanistic basis for rescuing hypertrophic cardiomyopathy with myosin regulatory light chain phosphorylation. Cytoskeleton (Hoboken); DOI: 10.1002/cm.21854.

Linke WA (2000). Titin elasticity in the context of the sarcomere: force and extensibility measurements on single myofibrils. Adv Exp Med Biol 481, 179–202; discussion 203–206.

Linke WA & Fernandez JM (2002). Cardiac titin: molecular basis of elasticity and cellular contribution to elastic and viscous stiffness components in myocardium. J Muscle Res Cell Motil 23, 483–497.

Ma W, Childers M, Murray J, Moussavi-Harami F, Gong H, Weiss R, Daggett V, Irving T & Regnier M (2020). Myosin dynamics during relaxation in mouse soleus muscle and modulation by 2′-deoxy-ATP. The Journal of Physiology 598, 5165–5182.

Ma W, Gong H & Irving T (2018). Myosin Head Configurations in Resting and Contracting Murine Skeletal Muscle. International Journal of Molecular Sciences 19, 2643.

Ma W, Henze M, Anderson RL, Gong H, Wong FL, del Rio CL & Irving T (2021). The Super-Relaxed State and Length Dependent Activation in Porcine Myocardium. Circulation Research 129, 617–630.

Ma W & Irving TC (2022). Small Angle X-ray Diffraction as a Tool for Structural Characterization of Muscle Disease. International Journal of Molecular Sciences 23, 3052.

Ma W, McMillen TS, Childers MC, Gong H, Regnier M & Irving T (2023). Structural OFF/ON transitions of myosin in relaxed porcine myocardium predict calcium-activated force. Proc Natl Acad Sci U S A 120, e2207615120.

Markandran K, Poh JW, Ferenczi MA & Cheung C (2021). Regulatory Light Chains in Cardiac Development and Disease. Int J Mol Sci 22, 4351.

Markandran K, Yu H, Song W, Lam DTUH, Madathummal MC & Ferenczi MA (2022). Functional and Molecular Characterisation of Heart Failure Progression in Mice and the Role of Myosin Regulatory Light Chains in the Recovery of Cardiac Muscle Function. International Journal of Molecular Sciences 23, 88.

Miller MS, Bedrin NG, Ades PA, Palmer BM & Toth MJ (2015). Molecular determinants of force production in human skeletal muscle fibers: effects of myosin isoform expression and cross-sectional area. Am J Physiol Cell Physiol 308, C473–484.

Moore JR, Campbell SG & Lehman W (2016). Structural determinants of muscle thin filament cooperativity. Arch Biochem Biophys 594, 8–17.

Mulieri LA, Barnes W, Leavitt BJ, Ittleman FP, LeWinter MM, Alpert NR & Maughan DW (2002). Alterations of myocardial dynamic stiffness implicating abnormal crossbridge function in human mitral regurgitation heart failure. Circ Res 90, 66–72.

Palmer BM, Suzuki T, Wang Y, Barnes WD, Miller MS & Maughan DW (2007). Two-state model of acto-myosin attachment-detachment predicts C-process of sinusoidal analysis. Biophys J 93, 760–769.

Perike S et al. (2023). Myosin Light Chain Dephosphorylation by PPP1R12C Promotes Atrial Hypocontractility in Atrial Fibrillation. bioRxiv2023.04.19.537590.

Pulcastro HC, Awinda PO, Breithaupt JJ & Tanner BCW (2016). Effects of myosin light chain phosphorylation on length-dependent myosin kinetics in skinned rat myocardium. Archives of Biochemistry and Biophysics 601, 56–68.

Scruggs SB, Hinken AC, Thawornkaiwong A, Robbins J, Walker LA, de Tombe PP, Geenen DL, Buttrick PM & Solaro RJ (2009). Ablation of Ventricular Myosin Regulatory Light

Chain Phosphorylation in Mice Causes Cardiac Dysfunction in Situ and Affects Neighboring Myofilament Protein Phosphorylation*. Journal of Biological Chemistry 284, 5097–5106.

Scruggs SB & Solaro RJ (2011). The significance of regulatory light chain phosphorylation in cardiac physiology. Arch Biochem Biophys 510, 129–134.

Shiels HA & White E (2008). The Frank-Starling mechanism in vertebrate cardiac myocytes. J Exp Biol 211, 2005–2013.

Siemankowski RF, Wiseman MO & White HD (1985). ADP dissociation from actomyosin subfragment 1 is sufficiently slow to limit the unloaded shortening velocity in vertebrate muscle. Proceedings of the National Academy of Sciences 82, 658–662.

Tanner BCW, Farman GP, Irving TC, Maughan DW, Palmer BM & Miller MS (2012). Thick-to-thin filament surface distance modulates cross-bridge kinetics in Drosophila flight muscle. Biophys J 103, 1275–1284.

Toepfer C, Caorsi V, Kampourakis T, Sikkel MB, West TG, Leung M-C, Al-Saud SA, MacLeod KT, Lyon AR, Marston SB, Sellers JR & Ferenczi MA (2013). Myosin regulatory light chain (RLC) phosphorylation change as a modulator of cardiac muscle contraction in disease. J Biol Chem 288, 13446–13454.

de Tombe PP, Mateja RD, Tachampa K, Ait Mou Y, Farman GP & Irving TC (2010). Myofilament length dependent activation. J Mol Cell Cardiol 48, 851–858.

Turner KL, Morris HS, Awinda PO, Fitzsimons DP & Tanner BCW (2023). RLC phosphorylation amplifies Ca2+ sensitivity of force in myocardium from cMyBP-C knockout mice. J Gen Physiol 155, e202213250.

Warren SA, Briggs LE, Zeng H, Chuang J, Chang EI, Terada R, Li M, Swanson MS, Lecker SH, Willis MS, Spinale FG, Maupin-Furlowe J, McMullen JR, Moss RL & Kasahara H (2012). Myosin Light Chain Phosphorylation Is Critical for Adaptation to Cardiac Stress. Circulation 126, 2575–2588.

Williams CD, Regnier M & Daniel TL (2010). Axial and radial forces of cross-bridges depend on lattice spacing. PLoS Comput Biol 6, e1001018.

Yadav S & Szczesna-Cordary D (2017). Pseudophosphorylation of cardiac myosin regulatory light chain: a promising new tool for treatment of cardiomyopathy. Biophys Rev 9, 57–64.

Yang Z, Stull JT, Levine RJC & Sweeney HL (1998). Changes in Interfilament Spacing Mimic the Effects of Myosin Regulatory Light Chain Phosphorylation in Rabbit Psoas Fibers. Journal of Structural Biology 122, 139–148.

Key Points

- Myosin regulatory light chain (RLC) is a thick-filament protein in the cardiac sarcomere that can be phosphorylated (RLC-P), and changes in RLC-P are associated with cardiac dysfunction and disease.
- This study assesses how RLC-P alters cardiac muscle structure and function at different sarcomere lengths and calcium concentrations.
- At low, non-activating levels of Ca^{2+}, RLC-P contributed to myofilament disorder, though there were no effects on isometric stress production and viscoelastic stiffness.
- With increases in sarcomere length and Ca^{2+}-activation, the structural changes due to RLC-P become greater, which translates into greater force production, greater viscoelastic stiffness, slower myosin detachment rate, and altered cross-bridge nucleotide handling rates.
- This work elucidates the role of RLC-P in regulating muscle function and facilitates understanding of thick-filament regulatory protein contributions to cardiac function in health and disease

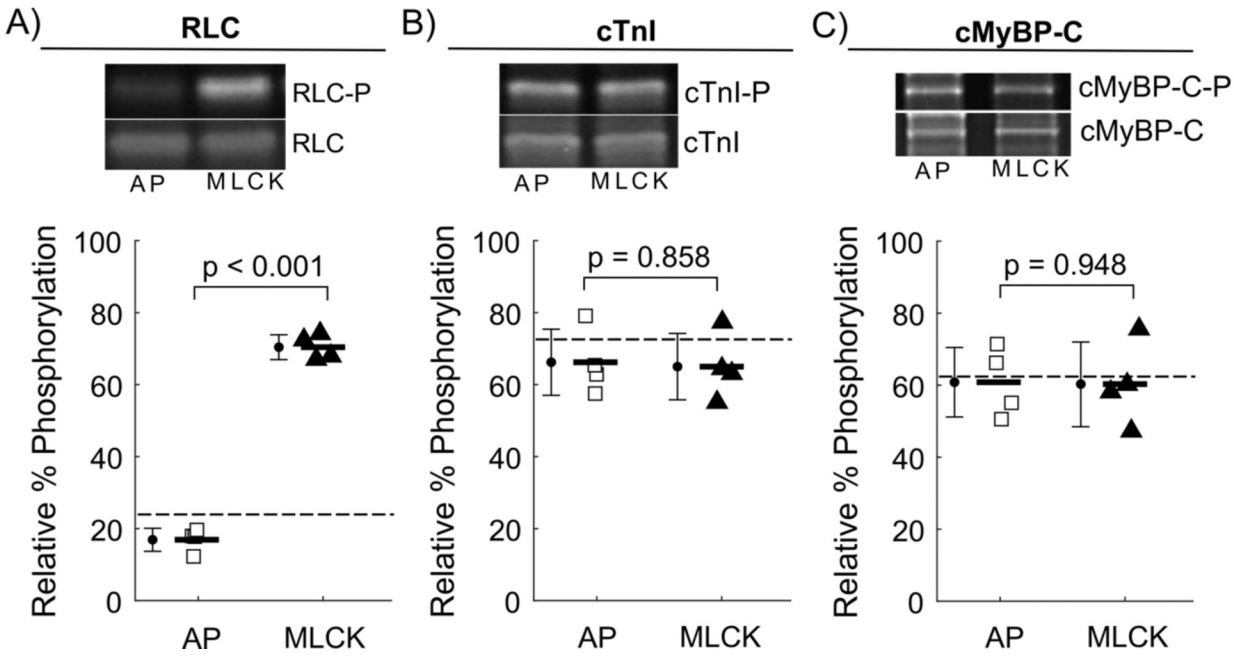

Figure 1.

AP and MLCK treatment of myocardial strips only affected RLC phosphorylation levels. Relative phosphorylation levels for the primary phosphorylatable myofilament regulatory proteins: A) regulatory light chain (RLC), B) cardiac troponin I (cTnI), and C) cardiac myosin binding protein-C (cMyBP-C) were quantified by SYPRO Ruby and Pro-Q Diamond gel stain. Average values represent mean±SD, using the with individual data points for each condition within each panel. Dashed lines represent untreated phosphorylation levels for each protein. Significance is listed within each panel. $n_{samples} = 2$ per condition (pooled from $n_{fibers} = 4$, technical replicates) from each heart ($n_{hearts} = 2$, biological replicates).

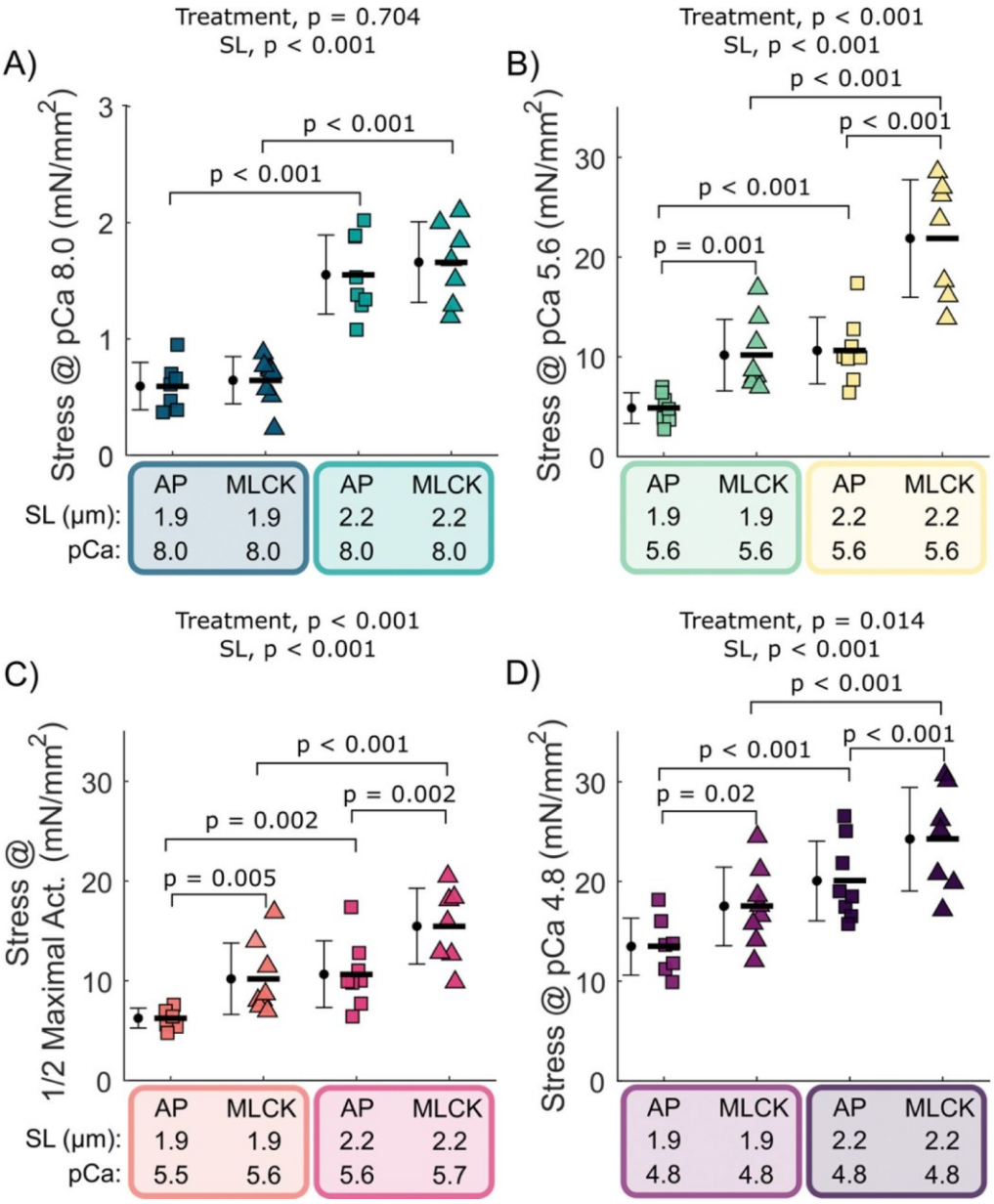

Figure 2: Regulatory light chain phosphorylation (RLC-P) increases active stress at short (1.9 µm) and long (2.2 µm) sarcomere lengths.

Summary data are shown for A) passive stress at pCa 8.0, B) active stress at pCa 5.6, C) active stress at ½ maximal activation, and D) active stress at pCa 4.8 for each condition. Averages represent mean±SD, with individual data points shown. Fixed effects are listed above each panel. Post-hoc comparisons are listed within each panel. n_{fibers} = 3–4 per condition (technical replicates) from each heart (n_{hearts} = 2, biological replicates).

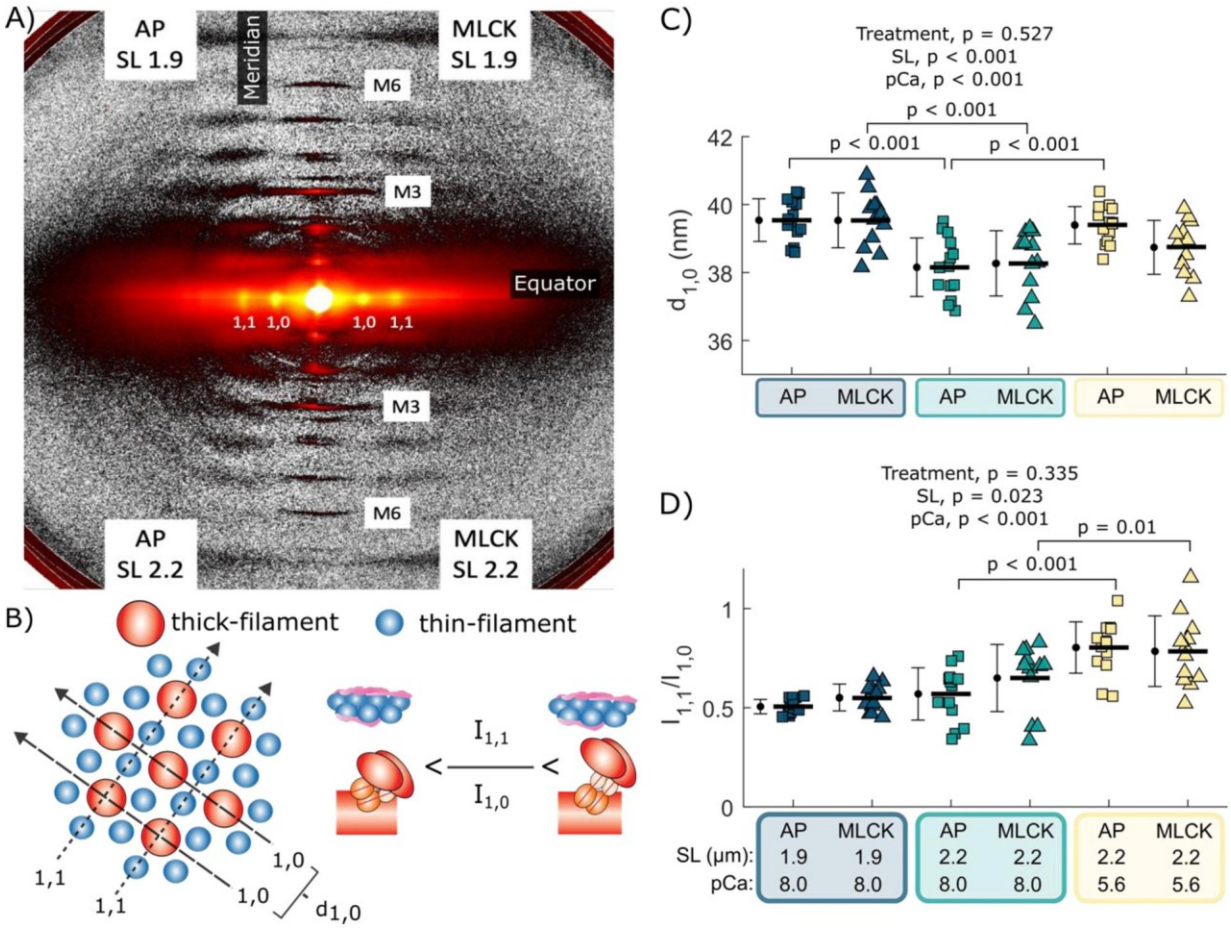

Figure 3: RLC-P does not alter equatorial parameters measured by small-angle x-ray diffraction.

A) Representative x-ray diffraction images of permeabilized porcine myocardium at low calcium (pCa 8.0) after treatment with AP or MLCK at sarcomere length 1.9 μm or 2.2 μm. Each quadrant shows a representative image for each of the conditions. Left: AP treatment; Right: MLCK treatment; Upper: SL 1.9 μm; Lower: SL 2.2 μm. B) The equatorial reflections are associated with thick- and thin-filament configuration. The 1,0 reflection arises from thick-filament mass, while the 1,1 reflection arises from both thick- and thin-filament mass. Increases in the equatorial intensity ratio, $I_{1,1}/I_{1,0}$, indicate movement of the myosin heads, with myosin head mass shifting away from the thick-filament backbone and toward the thin-filament. Summary data for C) thick- to thick- filament spacing ($d_{1,0}$), D) $I_{1,1}/I_{1,0}$. Averages represent mean± SD, with individual data points shown. Fixed effects are listed above each panel. Post-hoc comparisons are listed within each panel. n_{fibers} = 5–6 per condition (technical replicates) from each heart (n_{hearts} = 2, biological replicates).

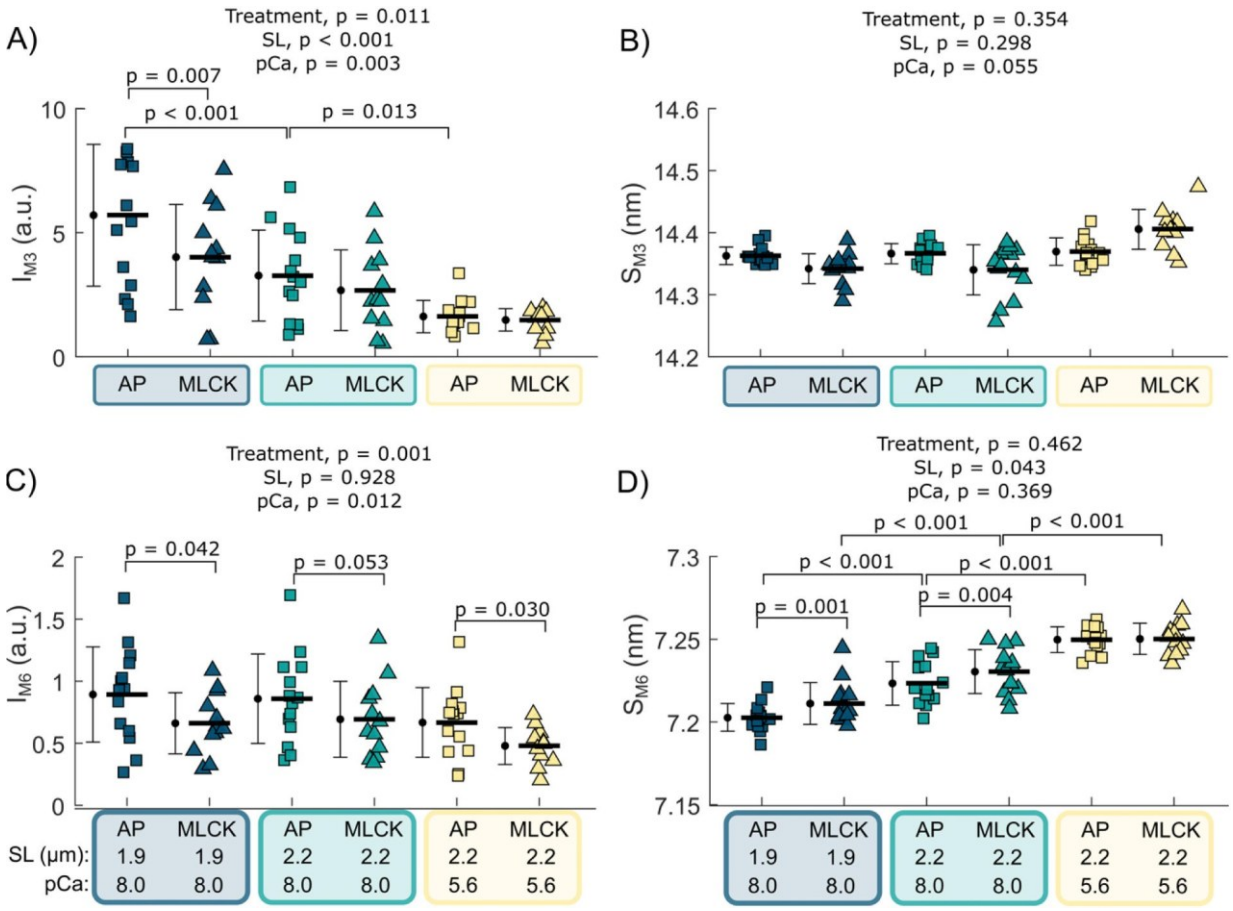

Figure 4: RLC-P influences meridional diffraction parameters associated with structural changes along the thick-filament backbone.

The meridional reflections are associated with the orientation and/or organization of myosin heads along the thick-filament backbone. Summary data for A) intensity of the third-order meridional reflection (I_{M3}), B) spacing of the third-order meridional reflection (S_{M3}), C) intensity of the sixth-order meridional reflection (I_{M6}), D) and spacing of the sixth-order meridional reflection (S_{M6}). Averages represent mean± SD, with individual data points shown. Fixed effects are listed above each panel. Post-hoc comparisons are listed within each panel. n_{fibers} = 5–6 per condition (technical replicates) from each heart (n_{hearts} = 2, biological replicates).

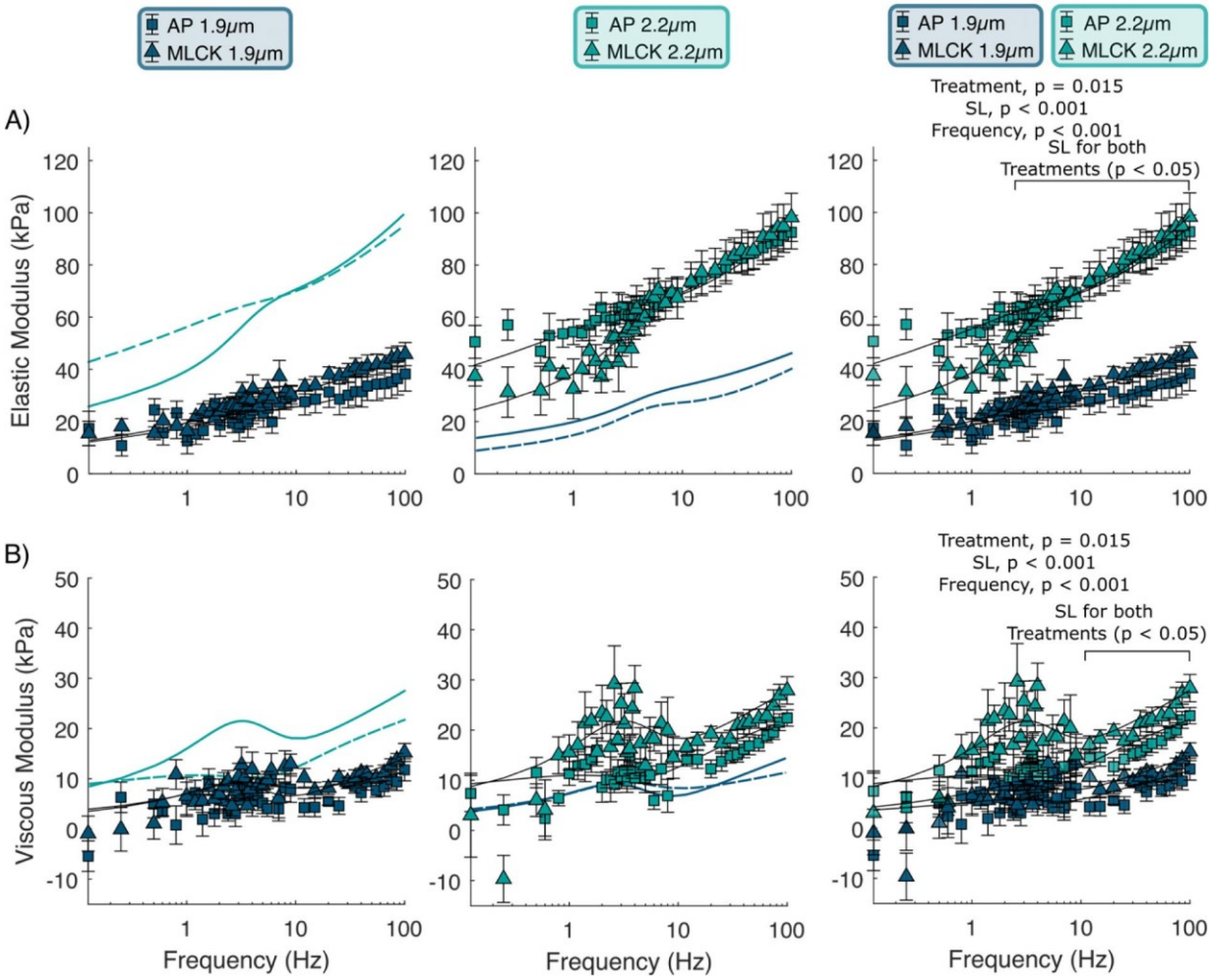

Figure 5: RLC-P does not affect passive viscoelastic stiffness at low [Ca^{2+}] (pCa 8.0).

A) Elastic and B) viscous moduli are plotted against oscillatory frequency from sinusoidal length-perturbation measurements. Averages represent mean±SEM. In the left and middle column, colored solid lines (=AP treatment) and dashed lines (=MLCK treatment) represent fit lines from the SL not shown on the panel. Fixed effects are listed above each right-most panel because the statistical analysis of the nested linear mixed model was only applied to all data (not sub-divided sections of data shown in the left and middle panels). Post-hoc comparisons are indicated within each right-most panel. n_{fibers} = 3–4 per condition (technical replicates) from each heart (n_{hearts} = 2, biological replicates).

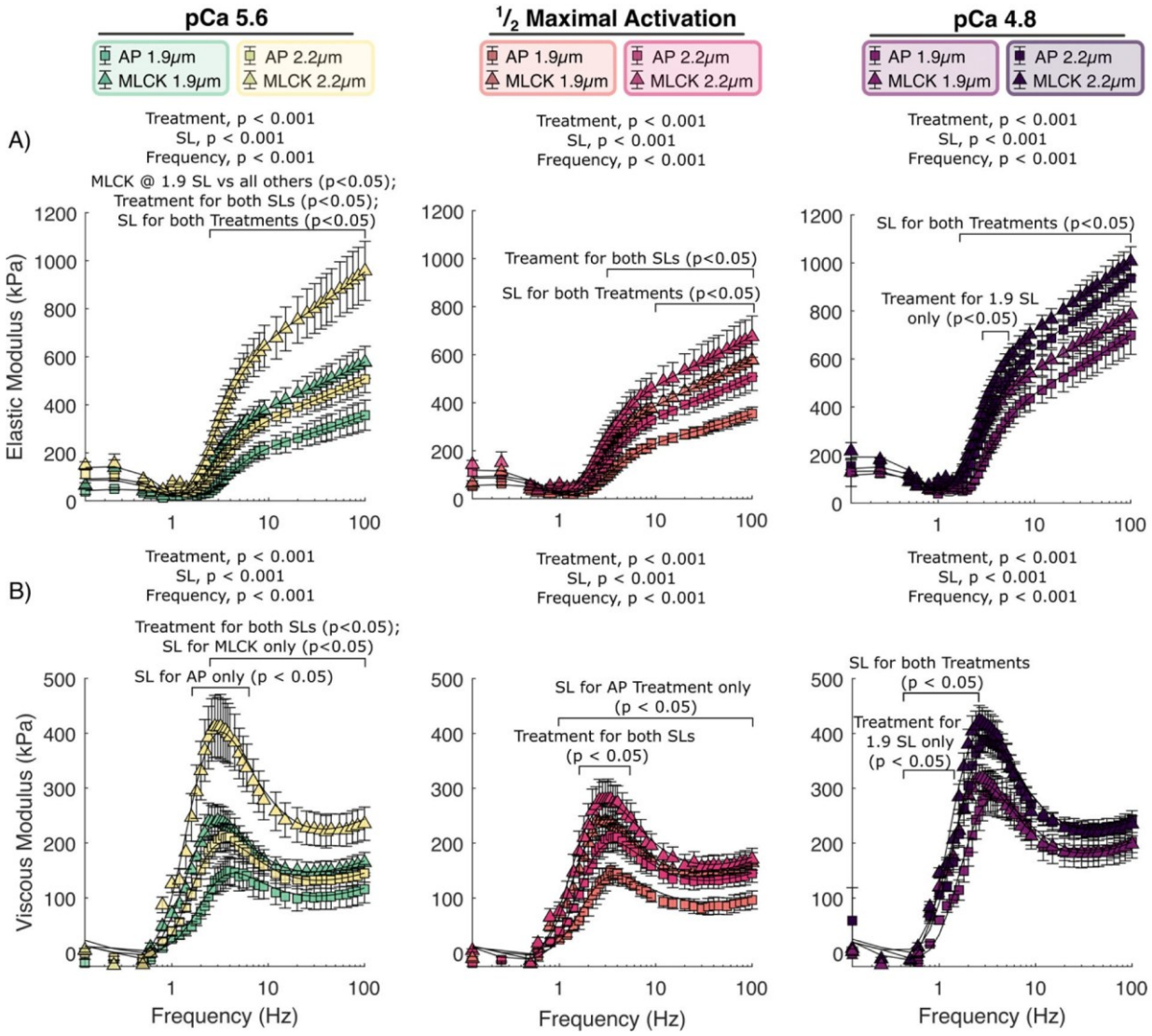

Figure 6: RLC-P and sarcomere length increase viscoelastic stiffness.

Elastic (A) and viscous moduli (B) are plotted against oscillatory frequency from sinusoidal length-perturbation measurements at pCa 5.6 (left column) and ½ maximal activation (middle column), and pCa 4.8 (right column). Fixed effects are listed above each panel. Averages represent mean±SEM. Post-hoc comparisons are listed within each panel. n_{fibers} = 3–4 per condition (technical replicates) from each heart (n_{hearts} = 2, biological replicates).

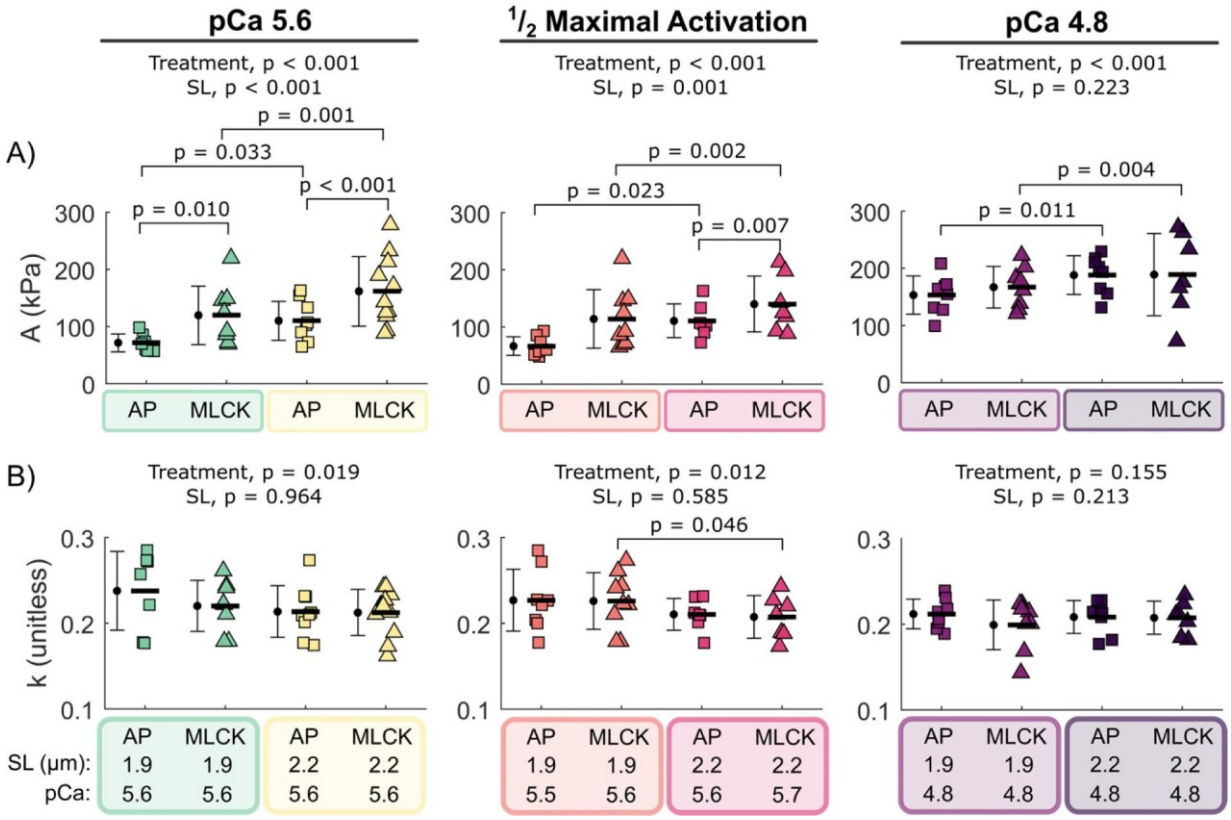

Figure 7: RLC-P increases cross-bridge stiffness or number of strongly bound cross-bridges. Summary data for parameters A (A), and k (B) at pCa 5.6 (left column), ½ maximal activation (middle column), and pCa 4.8 (right column). Fixed effects are listed above each panel. Averages represent mean± SD. Post-hoc comparisons are listed within each panel. n_{fibers} = 3–4 per condition (technical replicates) from each heart (n_{hearts} = 2, biological replicates).

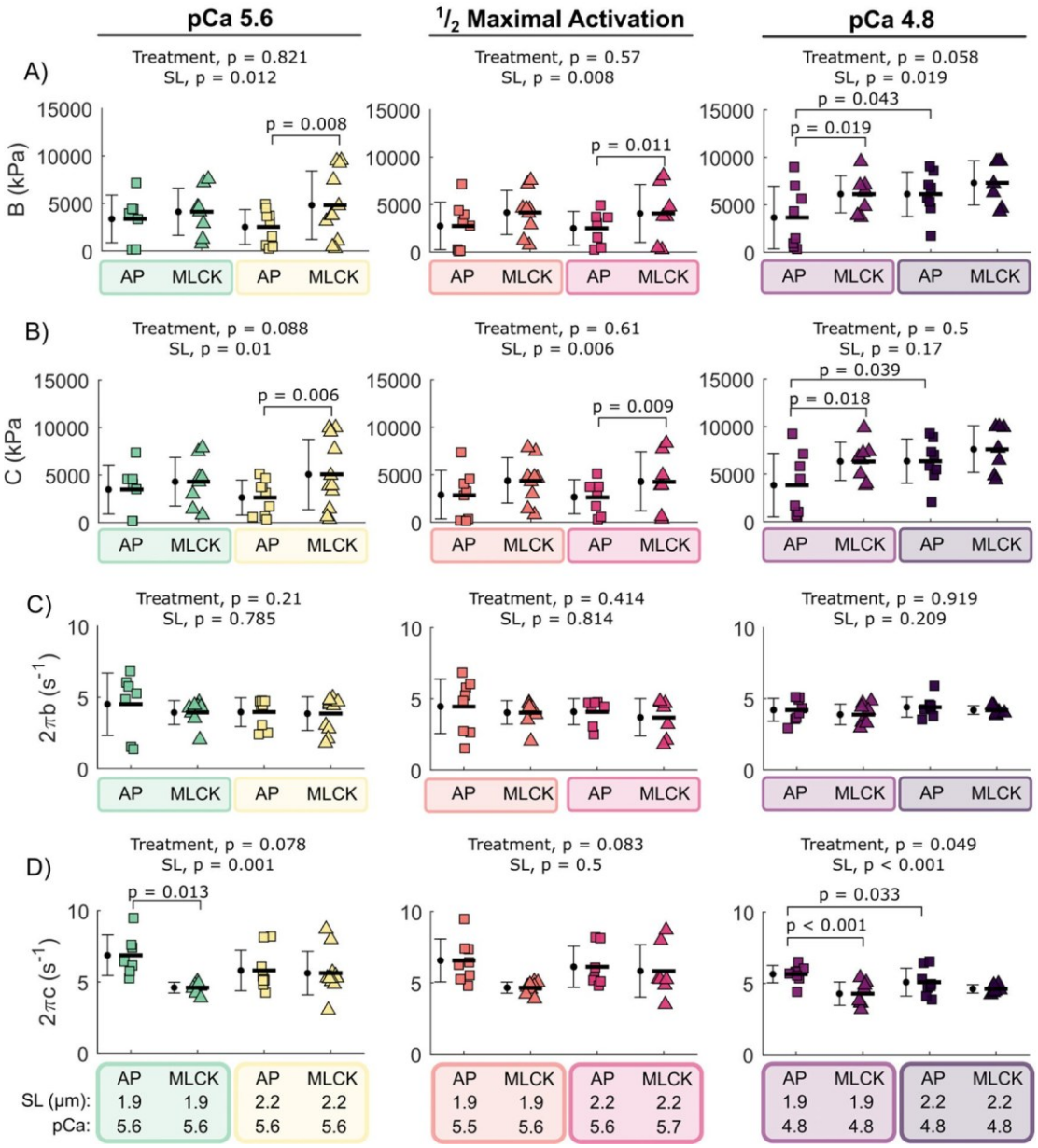

Figure 8: RLC-P decreases myosin head detachment rate.

Summary data for parameters B (A), C (B), 2πb (C), and 2πc (D) at pCa 5.6 (left column), ½ maximal activation (middle column), and pCa 4.8 (right column). Fixed effects are listed above each panel. Averages represent mean± SD. Post-hoc comparisons are listed within each panel. n_{fibers} = 3–4 per condition (technical replicates) from each heart (n_{hearts} = 2, biological replicates).

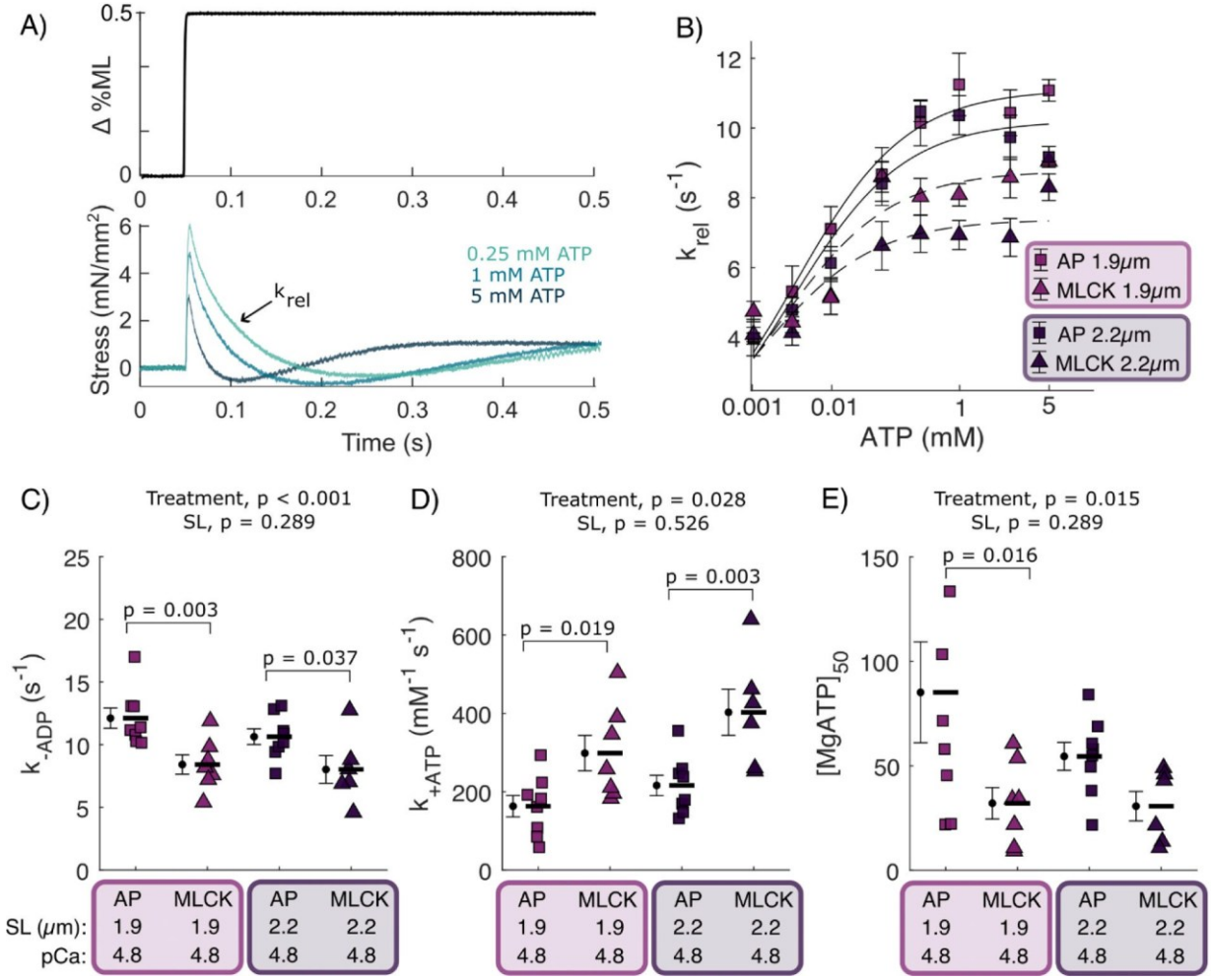

Figure 9: RLC-P decreases the ADP dissociation rate and increases the ATP association rate at both sarcomere lengths (pCa 4.8).

A) Permeabilized myocardial strips were stretched by 0.5% muscle length (ML, upper panel) and the stress response was measured as [ATP] was titrated to from 5 mM towards rigor (lower panel). B) k_{rel} vs [ATP] were fit to Eq. 2 to extract parameters that describe nucleotide handling rates for each experimental condition: C) k_{-ATP}, the ATP dissociation rate, and E) k_{+ATP}, the ATP association rate. F) $[MgATP]_{50}$, the MgATP concentration at half-maximal detachment rate for each condition. Averages represent mean± SD, with individual data points shown where applicable. Post-hoc comparisons are listed within each panel. n_{fibers} = 3–4 per condition (technical replicates) from each heart (n_{hearts} = 2, biological replicates).